Nationaal Lucht- en Ruimtevaartlaboratorium
National Aerospace Laboratory NLR

Executive summary

Multigrid Optimization for Space-Time Discontinuous Galerkin Discretizations of Advection Dominated Flows

Problem area
With the increasing demand of the aerospace industry for more accurate predicions of the flow around aircraft, the scientific community is developing higher-order numerical methods. The discontinuous Galerkin finite element method provides an easy framework for obtaining arbitrarily high order of accuracy. Combined with local grid refinement, the method even promises to be computationally more effective than classical second-order methods. Whereas there are numerous applications demonstrating the effectiveness of the method in terms of degrees of freedom, the *solution* of the discrete system still requires (significantly) more computational resources than classical methods do.

Description of work
This report concerns the development of efficient multigrid algorithms for the solution of the discrete equations obtained from a higher-order discontinuous Galerkin discretization of the Euler equations. The important benefit of multigrid algorithms is that they retain the local properties of the discontinuous Galerkin method and that they are memory efficient. The multigrid algorithm is developed in a semi-automatic way by optimizing the coefficients of the multigrid smoother in Fourier space. In this paper, explicit diagonal and full Runge-Kutta smoothers are considered.

Results and conclusions
Excellent multigrid performance has been obtained for the convection-diffusion equation. Unfortunately, the same smoothers applied to the nonlinear Euler equations did not show the same efficiency. This is most probably due to bad smoothing of the medium-frequency error modes. The development of efficient multigrid algorithms for the Euler equations will require a different class of smoothers than the one considered in this report.

Applicability
Efficient multigrid solvers are a prerequisite for large-scale and accurate simulation of flow problems with the discontinuous Galerkin method. Once these solvers are available, discontinuous Galerkin methods will be competitive methods.

Report no.
NLR-TP-2010-531

Author(s)
S. Rhebergen
J.J.W. van der Vegt
H. van der Ven

Report classification
UNCLASSIFIED

Date
February 2011

Knowledge area(s)
Computational Physics en theoretische aërodynamica

Descriptor(s)
discontinuous Galerkin
multigrid
convection-dominated flows

This report is a chapter in Notes on Numerical Fluid Mechanics and Multidisciplinary Design, Volume 113: ADIGMA: A European initiative on the development of adaptive higher-order variational methods for aerospace application, by N. Kroll et al (eds.).

Multigrid Optimization for Space-Time Discontinuous Galerkin Discretizations of Advection Dominated Flows

Nationaal Lucht- en Ruimtevaartlaboratorium, National Aerospace Laboratory NLR

Anthony Fokkerweg 2, 1059 CM Amsterdam,
P.O. Box 90502, 1006 BM Amsterdam, The Netherlands
Telephone +31 20 511 31 13, Fax +31 20 511 32 10, Web site: www.nlr.nl

Nationaal Lucht- en Ruimtevaartlaboratorium
National Aerospace Laboratory NLR

NLR-TP-2010-531

Multigrid Optimization for Space-Time Discontinuous Galerkin Discretizations of Advection Dominated Flows

S. Rhebergen[1], J.J.W. van der Vegt[1] and H. van der Ven

[1] Twente University

This report is a chapter in Notes on Numerical Fluid Mechanics and Multidisciplinary Design, Volume 113: ADIGMA: A European initiative on the development of adaptive higher-order variational methods for aerospace application, by N. Kroll et al (eds.). The work described in this report is partially funded by the EU project ADIGMA, and partially by NLR's programmatic research.

This publication has been refereed by the Advisory Committee AEROSPACE VEHICLES.

Customer	National Aerospace Laboratory NLR
Contract number	----
Owner	National Aerospace Laboratory NLR
Division NLR	Aerospace Vehicles
Distribution	Unlimited
Classification of title	Unclassified
	February 2011

Approved by:

Author	Reviewer	Managing department
16/3/2011	16/3/2011	17/3/2011

Summary

The goal of this research is to optimize multigrid methods for higher order accurate space-time discontinuous Galerkin discretizations. The main analysis tool is discrete Fourier analysis of two- and three-level multigrid algorithms. This gives the spectral radius of the error transformation operator which predicts the asymptotic rate of convergence of the multigrid algorithm. In the optimization process we therefore choose to minimize the spectral radius of the error transformation operator. We specifically consider optimizing h-multigrid methods with explicit Runge-Kutta type smoothers for second and third order accurate space-time discontinuous Galerkin finite element discretizations of the 2D advection-diffusion equation. The optimized schemes are compared with current h-multigrid techniques employing Runge-Kutta type smoothers. Also, the efficiency of h-, p- and hp-multigrid methods for solving the Euler equations of gas dynamics with a higher order accurate space-time DG method is investigated.

Contents

1 Table

4 Figures

(17 pages in total)

1 Introduction

Space-time discontinuous Galerkin (DG) discretizations of time-dependent partial differential equations result in a system of (non)-linear algebraic equations which can be solved efficiently with multigrid methods. In this paper we will discuss the optimization of multigrid techniques for higher order accurate space-time DG discretizations describing advection dominated flows. This research is a continuation of Ref. 3, 7 where we presented a multigrid algorithm in combination with a pseudo-time integration method for second order accurate space-time DG discretizations of the compressible Euler and Navier-Stokes equations. The main benefits of this multigrid algorithm are that no large global linear system needs to be solved and, through the use of Runge-Kutta type smoothers, the locality of the DG discretization is preserved. The algorithm is easy to implement and parallelize, even on locally refined meshes, and insensitive to initial conditions. For higher order accurate space-time DG discretizations the multigrid performance was, however, not satisfactory. The objective of this paper is to discuss improvements in the computational performance of space-time DG discretizations when higher order polynomial basis functions are used. The main tool to analyze the multigrid performance is three-level discrete Fourier analysis. This analysis tool is used to optimize the multigrid performance by minimizing the spectral radius of the multigrid error transformation operator. In particular, the focus will be on searching for better coefficients in the multigrid smoothing operator. More detailed information on the multigrid algorithms and the analysis techniques used in this paper can be found in e.g. Ref. 1, 6, 10, 11.

The outline of this paper is as follows. After a brief introduction in Chapter 2 on the multigrid error transformation operator, a summary of the discrete Fourier analysis of the multigrid algorithm will be given in Chapter 3. Next, we discuss the optimization of the multigrid algorithm in Chapter 4. Results of the optimization process will be given in Chapter 5 as well as a comparison in efficiency between h-, p- and hp-multigrid methods. Finally, conclusions are drawn in Chapter 6.

2 Multigrid error transformation operator

The main goal of the multigrid algorithm is to iteratively solve in an efficient way a system of (non)-linear algebraic equations $L_h v_h = f_h$ on a mesh $\mathcal{M}_h$, with L_h a linear or non-linear discretization operator and f_h a given right hand side. In the *h*-multigrid method we use a finite sequence N_c of increasingly coarser meshes $\mathcal{M}_{nh}$, $n \in \{1, \cdots, N_c\}$ to generate approximations

to the original problem. In addition, the data on the different meshes are connected with restriction operators $R_{nh}^{mh} : \mathcal{M}_{nh} \rightarrow \mathcal{M}_{mh}$ and prolongation operators $P_{mh}^{nh} : \mathcal{M}_{mh} \rightarrow \mathcal{M}_{nh}$, with $1 \leq n < m \leq N_c$. On these meshes a set of auxiliary problems is solved $\mathcal{M}_{nh}$, $1 < n \leq N_c$, namely $L_{nh}v_{nh} = f_{nh}$, in order to accelerate convergence. For non-linear problems we use the Full Approximation Scheme (FAS), see e.g. Ref. 6, but in the analysis of the multigrid performance we only consider linear problems.

In order to understand the performance of the multigrid algorithm we need to consider the multigrid error transformation operator. Given an initial error e_h^A, the error e_h^D after one full multigrid cycle with three grid levels is given by the relation

$$e_h^D = M_h^{3g} e_h^A$$

with

$$M_h^{3g} = S_h^{\nu_2}(I_h - P_{2h}^h(I_{2h} - M_{2h}^{\gamma_c})L_{2h}^{-1}R_h^{2h}L_h)S_h^{\nu_1} \tag{1}$$

and

$$M_{2h} = S_{2h}^{\nu_4}(I_{2h} - P_{4h}^{2h}L_{4h}^{-1}R_{2h}^{4h}L_{2h})S_{2h}^{\nu_3}. \tag{2}$$

Here, S_{nh} and I_{nh} are, respectively, the smoothing and identity operator on the mesh $\mathcal{M}_{nh}$, ν_i, $i = 1, \cdots, 4$, the number of pre- and post-smoothing iterations and γ_c the cycle index. In the multigrid analysis and computations we will also consider the effect of solving the algebraic system on the coarsest mesh approximately using ν_c smoother iterations instead of using an exact inverse. Next to *h*-multigrid also *p*-multigrid methods are possible in which on a single mesh coarser approximations are obtained by using lower order discretizations. Of course, combinations of both techniques are possible resulting in *hp*-multigrid methods.

3 Three-level multigrid analysis

3.1 Discrete Fourier analysis

Consider the infinite mesh G_h, which is defined as

$$G_h := \left\{x = (x_1, x_2) = (k_1h_1, k_2h_2) \mid k \in \mathbb{Z}^2, h \in \left(\mathbb{R}^+\right)^2\right\}.$$

On G_h we define for $v_h : G_h \rightarrow \mathbb{C}$ the norm

$$\|v_h\|_{G_h}^2 := \lim_{N\rightarrow\infty} \frac{1}{4N^2} \sum_{|k|\leq m} |v_h(kh)|^2,$$

where $|k| = \max\{|k_1|, |k_2|\}$. In the theoretical analysis we only consider linear problems, where the linear systems on the various meshes are described using stencil notation

$$L_{nh}v_{nh}(x) = \sum_{k \in J_n} l_{n,k} v_{nh}(x + kh), \qquad x \in G_{nh}, \tag{3}$$

with stencil coefficients $l_{n,k} \in \mathbb{R}^{m_k \times m_k}$ and finite index sets $J_n \subset \mathbb{Z}^2$ describing the stencil. The restriction operators R_{nh}^{mh}, prolongation operators P_{mh}^{nh} and smoothing operators S_{nh} with $1 \leq n < m \leq N_c$ are also expressed using stencil notation, see e.g. Ref. 6, 10, 11.

On the infinite mesh G_h, we define for $x \in G_h$ the continuous Fourier modes with frequency $\theta = (\theta_1, \theta_2) \in \mathbb{R}^2$ as $\phi_h(\theta, x) := e^{i\theta \cdot x/h}$ with $\theta \cdot x/h := \theta_1 x_1/h_1 + \theta_2 x_2/h_2$, $h \in (\mathbb{R}^+)^2$ and $i = \sqrt{-1}$. We also define the space of bounded infinite grid functions by $\mathcal{F}(G_h) := \{v_h \,|\, v_h : G_h \to \mathbb{C} \text{ with } \|v_h\|_{G_h} < \infty\}$. For each $v_h \in \mathcal{F}(G_h)$ there exists a Fourier transformation, hence $v_h(x)$ can be written as a linear combination of Fourier components

$$v_h(x) = \int_{|\theta| \leq \pi} \widehat{v_h}(\theta) e^{i\theta \cdot x/h} d\theta, \qquad x \in G_h, \tag{4}$$

with $x/h := (x_1/h_1, x_2/h_2) = j \in \mathbb{Z}^2$, and inverse transformation

$$\widehat{v_h}(\theta) = \frac{1}{4\pi^2} \sum_{x \in G_h} v_h(x) e^{-i\theta \cdot x/h}, \qquad -\pi \leq \theta_j < \pi,$$

see e.g. Ref. 1. Due to aliasing, Fourier components with $|\hat{\theta}| := \max\{|\theta_1|, |\theta_2|\} \geq \pi$ are not visible on G_h. These modes coincide with $e^{i\theta \cdot x/h}$, where $\theta = \hat{\theta} \,(\mathrm{mod}\ 2\pi)$. Hence, the Fourier space $\mathcal{F} := \text{span}\left\{e^{i\theta \cdot x/h} \mid \theta \in \Theta = [-\pi, \pi)^2, x \in G_h\right\}$ contains any bounded infinite grid function.

3.2 Three-grid Fourier analysis

For the three-grid Fourier analysis we define the Fourier harmonics $\mathcal{F}_{4h}(\theta)$ as

$$\begin{aligned}
&\mathcal{F}_{4h}(\theta) := \text{span}\{\phi_h(\theta_\beta^\alpha, x) \mid \alpha \in \alpha_2, \beta \in \beta_2\}, \quad \text{where} \\
&\theta = \theta_0^0 \in \Theta_{4h} := [-\pi/4, \pi/4)^2, \\
&\theta_\beta = \theta_0^0 - (\bar{\beta}_1 \,\text{sign}\,(\theta_1), \bar{\beta}_2 \,\text{sign}\,(\theta_2))\pi, \\
&\theta_\beta^\alpha := \theta_\beta - (\bar{\alpha}_1 \text{sign}\,((\theta_1)_\beta), \bar{\alpha}_2 \,\text{sign}\,((\theta_2)_\beta))\pi, \\
&\alpha_2 := \{\alpha = (\bar{\alpha}_1, \bar{\alpha}_2) \mid \bar{\alpha}_i \in \{0, 1\}, i = 1, 2\} \\
&\beta_2 := \{\beta = (\bar{\beta}_1, \bar{\beta}_2) \mid \bar{\beta}_i \in \{0, \frac{1}{2}\}, i = 1, 2\}.
\end{aligned}$$

Note that we have 16 coupled Fourier harmonics, all related to θ_{00}^{00}. In the transition from G_{2h} to G_{4h} the modes $\theta_\beta = \theta_\beta^0$ are not visible due to aliasing.

The error e_h^D after one iteration of a three-grid multigrid cycle is determined by $e_h^D = M_h^{3g} e_h^A$, with e_h^A the initial error and M_h^{3g} the three-level multigrid error transformation operator defined by (1).

The properties of the error transformation operator can be investigated using discrete Fourier analysis. For this purpose we introduce the following matrices

$$\widehat{L}_h^{2g}(\theta_\beta) = \text{diag}\ (\widehat{L_h}(\theta_\beta^{00}), \widehat{L_h}(\theta_\beta^{11}), \widehat{L_h}(\theta_\beta^{10}), \widehat{L_h}(\theta_\beta^{01})) \in \mathbb{C}^{4m\times 4m} \tag{5}$$

$$\widehat{S}_h^{2g}(\theta_\beta) = \text{diag}\ (\widehat{S_h}(\theta_\beta^{00}), \widehat{S_h}(\theta_\beta^{11}), \widehat{S_h}(\theta_\beta^{10}), \widehat{S_h}(\theta_\beta^{01})) \in \mathbb{C}^{4m\times 4m} \tag{6}$$

$$\widehat{R}_h^{2g}(\theta_\beta) = (\widehat{R_h^{2h}}(\theta_\beta^{00}), \widehat{R_h^{2h}}(\theta_\beta^{11}), \widehat{R_h^{2h}}(\theta_\beta^{10}), \widehat{R_h^{2h}}(\theta_\beta^{01})) \in \mathbb{C}^{m\times 4m} \tag{7}$$

$$\widehat{P}_h^{2g}(\theta_\beta) = (\widehat{P_{2h}^{h}}(\theta_\beta^{00}), \widehat{P_{2h}^{h}}(\theta_\beta^{11}), \widehat{P_{2h}^{h}}(\theta_\beta^{10}), \widehat{P_{2h}^{h}}(\theta_\beta^{01}))^T \in \mathbb{C}^{4m\times m} \tag{8}$$

where diag refers to a diagonal matrix consisting of $m \times m$ blocks with $m \in \mathbb{N}$. The Fourier symbol of the linear operator L_{nh} is equal to $\widehat{L_{nh}}(\theta) = \sum_{k\in J_n} l_{n,k} e^{i\theta\cdot k}$. Similar expressions can be derived for the Fourier symbols of the restriction operator $\widehat{R_{nh}^{mh}}(\theta)$, the prolongation operator $\widehat{P_{mh}^{nh}}(\theta)$ and the smoothing operator $\widehat{S_{nh}}(\theta)$ on the various mesh levels. For more details, see e.g. Ref. 1, 6, 11. We also introduce the matrices

$$\widehat{L}_h^{3g}(\theta) = \text{bdiag}\ \big(\widehat{L}_h^{2g}(\theta_{00}), \widehat{L}_h^{2g}(\theta_{\frac{1}{2}\frac{1}{2}}), \widehat{L}_h^{2g}(\theta_{\frac{1}{2}0}), \widehat{L}_h^{2g}(\theta_{0\frac{1}{2}})\big) \in \mathbb{C}^{16m\times 16m}$$

$$\widehat{S}_h^{3g}(\theta) = \text{bdiag}\ \big(\widehat{S}_h^{2g}(\theta_{00}), \widehat{S}_h^{2g}(\theta_{\frac{1}{2}\frac{1}{2}}), \widehat{S}_h^{2g}(\theta_{\frac{1}{2}0}), \widehat{S}_h^{2g}(\theta_{0\frac{1}{2}})\big) \in \mathbb{C}^{16m\times 16m}$$

$$\widehat{R}_h^{3g}(\theta) = \text{bdiag}\ \big(\widehat{R}_h^{2g}(\theta_{00}), \widehat{R}_h^{2g}(\theta_{\frac{1}{2}\frac{1}{2}}), \widehat{R}_h^{2g}(\theta_{\frac{1}{2}0}), \widehat{R}_h^{2g}(\theta_{0\frac{1}{2}})\big) \in \mathbb{C}^{4m\times 16m}$$

$$\widehat{P}_h^{3g}(\theta) = \text{bdiag}\ \big(\widehat{P}_h^{2g}(\theta_{00}), \widehat{P}_h^{2g}(\theta_{\frac{1}{2}\frac{1}{2}}), \widehat{P}_h^{2g}(\theta_{\frac{1}{2}0}), \widehat{P}_h^{2g}(\theta_{0\frac{1}{2}})\big) \in \mathbb{C}^{16m\times 4m}$$

$$\widehat{Q}_h^{3g}(\theta) = \text{bdiag}\ \big(\widehat{L_{2h}^{-1}}(2\theta_{00}), \widehat{L_{2h}^{-1}}(2\theta_{\frac{1}{2}\frac{1}{2}}), \widehat{L_{2h}^{-1}}(2\theta_{\frac{1}{2}0}), \widehat{L_{2h}^{-1}}(2\theta_{0\frac{1}{2}})\big) \in \mathbb{C}^{4m\times 4m}.$$

The discrete Fourier transform of the error transformation operator for a three-level multigrid cycle $\widehat{M}_h^{3g}(\theta) \in \mathbb{C}^{16m\times 16m}$ then is equal to Ref. 11

$$\widehat{M}_h^{3g}(\theta) = \big(\widehat{S}_h^{3g}(\theta)\big)^{\nu_2}\Big(I^{3g} - \widehat{P}_h^{3g}(\theta)\widehat{U}^{3g}(\theta;\gamma_c)\widehat{Q}_h^{3g}(\theta)\widehat{R}_h^{3g}(\theta)\widehat{L}_h^{3g}(\theta)\Big)\big(\widehat{S}_h^{3g}(\theta)\big)^{\nu_1} \tag{9}$$

with I^{3g} the $16m \times 16m$ identity matrix and $\theta \in \Theta_{4h} \setminus \Psi_{3g}$, where Ψ_{3g} is defined as $\Psi_{3g} := \big\{\theta \in \Theta_{4h} \mid \widehat{L_{4h}}(4\theta_0^0) = 0 \text{ or } \widehat{L_{2h}}(2\theta_\beta^0) = 0 \text{ or } \widehat{L_h}(\theta_\beta^\alpha) = 0\big\}$. We still need to obtain an explicit expression for $\widehat{U}^{3g}(\theta;\gamma_c) \in \mathbb{C}^{4m\times 4m}$. On the mesh G_{2h} the modes θ_β^α reduce after the restriction operator to modes $2\theta_\beta^0$, hence using the result of a two-level analysis the coarse grid error transformation operator is equal to

$$\widehat{M}_{2h}^{2g}(2\theta_\beta) = \big(\widehat{S}_{2h}^{2g}(2\theta_\beta)\big)^{\nu_4}\Big(I^{2g} - \widehat{P}_{2h}^{2g}(2\theta_\beta)\widehat{L}_{4h}^{-1}(4\theta_0^0)\widehat{R}_{2h}^{2g}(2\theta_\beta)\widehat{L}_{2h}^{2g}(2\theta_\beta)\Big)\big(\widehat{S}_{2h}^{2g}(2\theta_\beta)\big)^{\nu_3},$$

with I^{2g} the $4m \times 4m$ identity matrix and $\theta_\beta \in \Theta_{2h} := [-\pi/4, \pi/4)^2 \setminus \Psi_{2g}$, where Ψ_{2g} is defined as $\Psi_{2g} := \{\theta \in [-\pi/4, \pi/4)^2 \mid \widehat{L_{4h}}(4\theta_0^0) = 0 \text{ or } \widehat{L_{2h}}(2\theta_\beta^0) = 0\}$. The matrices $\widehat{L}_{2h}^{2g}$, $\widehat{S}_{2h}^{2g}$, $\widehat{R}_{2h}^{2g}$ and $\widehat{P}_{2h}^{2g}$ are given by (5)-(8), respectively, with h replaced by $2h$. The matrix $\widehat{U}^{3g}(\theta; \gamma_c)$ then is equal to

$$\widehat{U}^{3g}(\theta; \gamma_c) = I^{2g} - \big(\widehat{M}_{2h}^{2g}(2\theta_\beta)\big)^{\gamma_c}.$$

The spectral radius of the error transformation operator gives a prediction of the asymptotic rate of convergence of the multigrid method. This asymptotic convergence is expressed in terms of the asymptotic convergence factor per cycle, which is equal to

$$\mu = \sup_{\theta \in \Theta_{3g} \setminus \Psi_{3g}} \rho\big(\widehat{M}^{3g}(\theta)\big), \tag{10}$$

with ρ is the spectral radius. A requirement for convergence of the multigrid algorithm is that the spectral radius satisfies the condition $\mu < 1$. By minimizing the spectral radius of the three-level multigrid error transformation operator (9), we obtain optimized multigrid algorithms.

4 Optimizing multigrid for space-time DG discretizations

The theory of the previous sections holds for general linear discretizations and smoothing operators, but in this paper we are specifically interested in designing optimized multigrid methods for higher order accurate space-time DG discretizations. For the optimization, we will consider the 2D advection-diffusion equation as model problem

$$\partial_t u + \vec{a} \cdot \nabla u - \nabla \cdot (\bar{\bar{A}} \nabla u) = 0, \quad x \in \Omega \subset \mathbb{R}^2,\ t \in \mathbb{R}^+, \tag{11}$$

where we assume that the advection velocity $\vec{a} \in \mathbb{R}^2$ and diffusion matrix $\bar{\bar{A}} \in (\mathbb{R}^+)^2$ are constant, with $\bar{\bar{A}}_{11} = \nu_x$, $\bar{\bar{A}}_{22} = \nu_y$ and $\bar{\bar{A}}_{12} = \bar{\bar{A}}_{21} = 0$. We do not discuss the details of the space-time DG discretization for the advection-diffusion equation, but refer to Ref. 3, 5 for more details. In the multigrid optimization we consider a uniform space-time mesh with elements $\Delta t \times \Delta x \times \Delta y$ and periodic boundary conditions. The discretization depends on the following dimensionless numbers:

$$CFL = \frac{a\Delta t}{h}, \quad Re_x = \frac{a(\Delta x)^2}{\nu_x h}, \quad Re_y = \frac{a(\Delta y)^2}{\nu_y h}, \quad AR = \frac{\Delta y}{\Delta x},$$

in which $h = \Delta x\sqrt{1 + AR^2}$ and $a = \sqrt{a_x^2 + a_y^2}$. Furthermore, we introduce the flow angle γ^{flow} with respect to the x-axis so that $a_x = \cos(\gamma^{flow})a$ and $a_y = \sin(\gamma^{flow})a$.

4.1 Pseudo-time integration and Runge-Kutta methods

The system of algebraic equations resulting from the space-time DG discretization of the 2D advection-diffusion equation can be represented as

$$\mathcal{L}(\hat{u}^n; \hat{u}^{n-1}) = 0, \tag{12}$$

with $\hat{u}^n$ the expansion coefficients of a polynomial approximation of u and n refers to the time index. To solve the system of coupled equations for the expansion coefficients $\hat{u}^n$ in (12), a pseudo time derivative is added to the system Ref. 7:

$$\Delta x \Delta y \frac{\partial \hat{u}^*}{\partial \tau} = -\frac{1}{\Delta t}\mathcal{L}(\hat{u}^*; \hat{u}^{n-1}), \tag{13}$$

which is integrated to steady-state in pseudo-time. At steady state, $\hat{u}^n = \hat{u}^*$. For the pseudo-time integration we introduce the dimensionless number $\lambda = \Delta\tau/\Delta t$ and use the pseudo-time CFL number, defined as $CFL^\tau = \lambda CFL$. To solve (13) we consider N-stage Runge-Kutta methods. For notational purposes, we set $\mathcal{L}(\hat{V}^*; u^{n-1}) = \mathcal{L}(\hat{V}^*)$. Initialize $\hat{V}^0 = \hat{u}^{n-1}$. Then, an N-stage Runge-Kutta scheme is given by:

$$(1 + \beta_j \lambda I)\hat{V}^j = \hat{V}^0 - \lambda\left(\sum_{l=1}^{j} \alpha_{j+1,l}\mathcal{L}(\hat{V}^{l-1})/(\Delta x \Delta y)\right) + \lambda\beta_j \hat{V}^{j-1}, \quad j = 1, ..., N,$$

with $\hat{u}^* = \hat{V}^N$. We see that there are a number of free parameters in the Runge-Kutta smoother. The smoother is therefore a good candidate for optimization. We will minimize the spectral radius (10) by optimizing the parameters α and β. In this paper only 5-stage Runge-Kutta schemes are considered for which we require that they are second order accurate in pseudo-time. This requirement gives constraints on the α coefficients. The β coefficients serve as the Melson correction to improve stability for small values of $\lambda \cong 1$, see Melson et al. Ref. 4.

4.2 Optimization results

We now provide some examples of the optimization of the Runge-Kutta (RK) smoothers for multigrid. We distinguish between diagonal RK schemes (dRK5) and full RK schemes (fRK5) in which all coefficients $\alpha_{j+1,l}$, with $1 \leq l \leq j \leq N$, are non-zero. We present optimized RK coefficients for the second ($p = 1$) and third ($p = 2$) order accurate space-time DG discretizations of the 2D advection-diffusion equation. For this we use the optimization procedures `fminsearch` and `fmincon`, available in Matlab. As constraint in the `fmincon` procedure, we require that both the spectral radius of the smoother and the three-level multigrid error transformation operator are less than 1. The optimization was performed for advection dominated steady flows in which we fix the Reynolds numbers $Re_x = Re_y = 100$ and the CFL number as $CFL = 100$. We also set the flow angle $\gamma^{flow} = \pi/4$, the aspect ratio $AR = 1$ and the number of pre- and

post-smoothing steps $\nu_1 = \nu_2 = 1$. On the coarsest grid, we use four smoother steps instead of an exact inverse. Furthermore, $\gamma = 1$. As initial guess in the optimization procedure, we use the EXI RK method Ref. 7 for the optimized dRK5 scheme. We then use the dRK5 scheme as initial guess to obtain the fRK5 scheme. The optimized coefficients and spectral radii of the smoother $\rho^{\mathcal{S}}$ and the 3-level multigrid operator ρ^{MG} are given in Table 1. As a comparison, we also give the spectral radius of the 3-level multigrid operator with EXI-RK smoother, ρ^{EXI-MG} when using the given parameters. We see that for these parameters the multigrid algorithm with the EXI smoother is very unstable, while good convergence can be achieved with our optimized schemes.

5 Testing multigrid performance

In this section we test the multigrid performance. We start in Section 5.1 by comparing the optimized h-multigrid algorithms of the previous sections to the original EXI-EXV h-multigrid method Ref. 3. For this we consider the 2D advection-diffusion equation. In Section 5.2 we consider a more complex test case in which we solve the Euler equations for inviscid flow over an NACA0012 airfoil. We will compare the performance of h-multigrid with p- and hp-multigrid.

5.1 The 2D advection-diffusion equation

In order to demonstrate the performance of the optimized algorithms we consider (11) on $\Omega = (0,1)^2$ with initial condition $u(x,y,0) = 1 - \frac{1}{2}(x+y)$ and boundary condition $u(x,y,t) = g(x,y)$. Here $g(x,y)$ equals at the domain boundary the exact steady state solution of (11) given by:

$$u(x,y) = \frac{1}{2}\left(\frac{\exp(a_1/\nu_x) - \exp(a_1 x/\nu_x)}{\exp(a_1/\nu_x) - 1} + \frac{\exp(a_2/\nu_y) - \exp(a_2 y/\nu_y)}{\exp(a_2/\nu_y) - 1}\right).$$

In the discretization we use a Shishkin mesh Ref. 3 which is suitable for dealing with boundary layers. The parameters in the test cases are the following: we consider a mesh with 32×32 elements, one physical time step, with $\Delta t = 100$, $a = \sqrt{2}$, $\nu_x = \nu_y = 0.01$ and a flow angle $\gamma^{flow} = \pi/4$. For the optimized RK schemes, we used a local pseudo-time scaling to deal with viscous flows Ref. 9. For the multigrid computations we use $\nu_i = 1,\ i = 1,2,3,4$ and $\gamma = 1$. On the coarsest mesh we investigate the effect of using $\nu_C = 4$ smoother iterations or solving the discrete system exactly.

In Figures 1 and 2, we show the convergence results of the different smoothers for 3-level multigrid. We see that in all cases a big improvement is obtained with the optimized Runge-Kutta smoothers over the original EXI-EXV smoother. For a second order accurate space-time DG

Table 1 Optimized coefficients for the dRK5 and fRK5 smoothers for 3-level multigrid for steady flows.

	dRK5 $p=1$	fRK5 $p=1$	dRK5 $p=2$	fRK5 $p=2$
α_{21}	0.057689952980	0.0578331573	0.048650095890	0.04877436325
α_{31}	-	-	-	-
		0.0002051554736		0.0002188348438
α_{32}	0.1405960888	0.1403808301	0.130316854	0.1300906122
α_{41}	-	0.0003953470071	-	2.608884832e-
				05
α_{42}	-	-	-	2.444376496e-
		0.001195029164		05
α_{43}	0.267958213	0.2681810517	0.2729621396	0.2734805705
α_{51}	-	0.0001441249202	-	-
				0.001250385487
α_{52}	-	-	-	-
		0.0002608610327		0.0007838720635
α_{53}	-	-	-	-
		0.0003368070181		0.0004890887712
α_{54}	0.5	0.8473374098	0.5	4.412139367
α_{61}	-	0.4115573097	-	0.8097217358
α_{62}	-	-	-	0.08435089009
		0.003144851878		
α_{63}	-	-	-	-
		0.0001096455683		0.01986799007
α_{64}	-	0.001555741114	-	0.01359815476
α_{65}	1.0	0.5901414466	1.0	0.1121972094
β_1	0.057689952980	0.04887040625	0.048650095890	0.5551936269
β_2	0.1405960888	0.1274785795	0.130316854	0.1333199239
β_3	0.267958213	0.2287556298	0.2729621396	-1.332263675
β_4	0.5	0.9547064029	0.5	-3.649588578
β_5	1.0	2.52621971	1.0	0.46771792
CFL^{τ}	0.8	0.8	0.4	0.4
$\rho^{\mathcal{S}}$	0.98812	0.98914	0.98974	0.9896
ρ^{MG}	0.89151	0.81762	0.90049	0.89903
ρ^{EXI-MG}	167.06	-	124.02	-

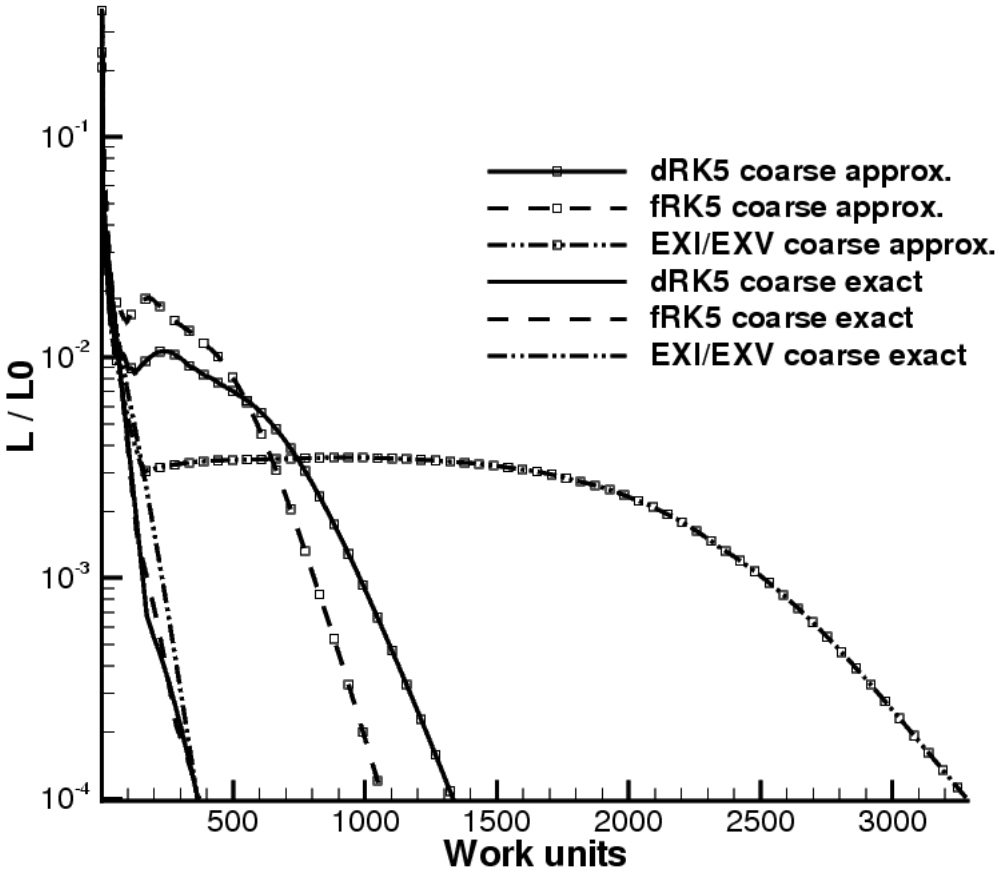

Fig. 1 Convergence results of second order space-time DG for three level multigrid algorithms with different Runge-Kutta smoothers. (dRK5, fRK5 and the EXI-EXV scheme Ref. 2, exact and approximate solution of equations on coarsest mesh).

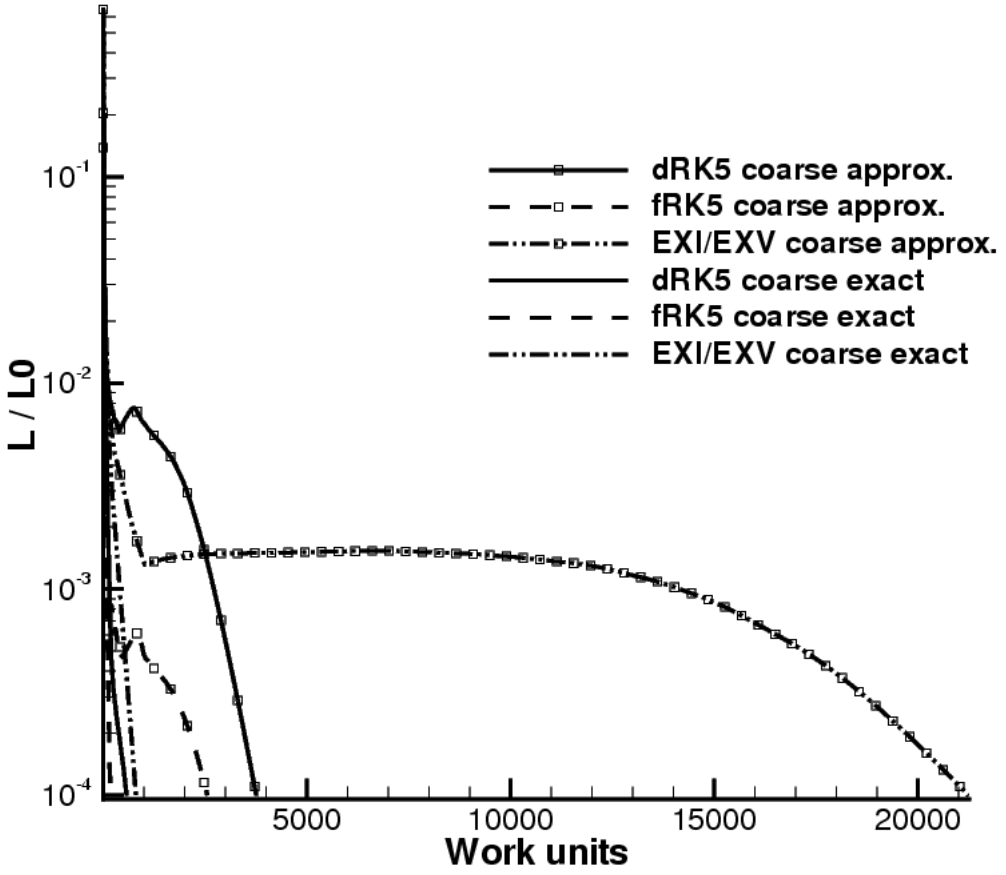

Fig. 2 Convergence results of third order space-time DG for three level multigrid algorithms with different Runge-Kutta smoothers. (dRK5, fRK5 and the EXI-EXV scheme Ref. 2, exact and approximate solution of equations on coarsest mesh).

discretization the number of multigrid cycles to obtain 4 orders of reduction in the residual is reduced from 3283 to 371. For the third order accurate DG discretization the number of multigrid cycles reduces from 21254 to 184. Furthermore, comparing dRK5 with fRK5, we see that the differences for a second order accurate space-time DG discretization is negligible. For a third order accurate space-time DG discretization this difference is, however, significant. Using more Runge-Kutta coefficients enlarges the possibilities to optimize the smoother.

The effect of solving the equations on the coarsest mesh with high accuracy is very large. Without this the multigrid convergence significantly slows down after a rapid initial decrease of the residual. In particular, for nonlinear problems it is tempting to solve the algebraic system on the coarsest mesh only approximately, because otherwise a global Newton solver is required. The effect of accurately solving the algebraic equations for the linear advection-diffusion equation on the coarsest mesh is, however, non-negligible.

5.2 The Euler equations

We now compare the performance of an h-multigrid method with p- and hp-multigrid. Since the difference between EXI and the optimized RK smoothers for the Euler equations is small we will only show the EXI results. As test case we consider 2D steady subsonic flow around a NACA0012 airfoil with an angle of attack of $\alpha = 2^\circ$ and far-field Mach number $Ma = 0.5$ (MTC1 test case). Since this test case is a steady-state flow problem, we consider a space-time DG discretization which is only first-order accurate in time but third-order accurate in space. The grid around the airfoil has 448×64 elements.

For single-grid, p- and hp-multigrid computations we used a pseudo-time CFL number of $CFL^\tau = 1.6$, while for h-multigrid $CFL^\tau = 0.8$. Larger pseudo-time CFL numbers for h-multigrid resulted in unstable calculations. For the p-multigrid method we solve the lowest order problem approximately taking $\nu_C = 20$. For the h- and hp-multigrid methods we solve the coarsest grid problem approximately, also taking $\nu_C = 20$. Furthermore, for the h-multigrid method, we also solve the coarse grid problem exactly using a matrix-free Newton method. In all cases, 5 pre- and post-smoothing steps were taken on each multigrid level. The Mach contours are given in Figure 3 while the convergence history plot is given in Figure 4.

We see that h-multigrid performs the worst while p- and hp-multigrid converge six orders in approximately the same amount of work units. We, however, had to take a twice as small CFL^τ number in the h-multigrid calculation compared to the other calculations. Furthermore, we see that after the high-frequency error modes have been smoothed, h-multigrid efficiency quickly deteriorates. A possible reason for this could be that the coarse-grid problem of the h-multigrid

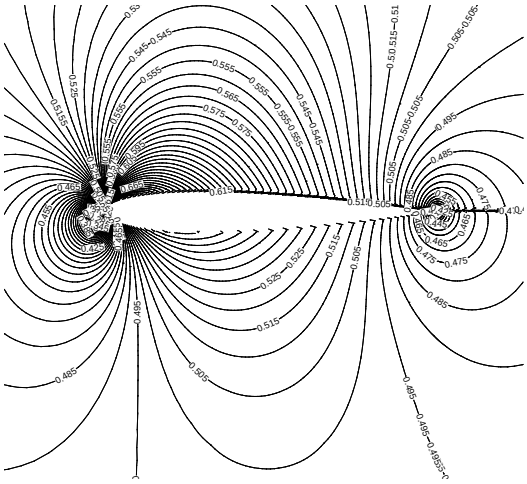

Fig. 3 Mach contours of inviscid flow around an NACA0012 airfoil ($\alpha = 2°, Ma = 0.5$).

algorithm is not solved well with respect to the characteristic components, see Ref. 12. We also see that there is hardly any difference in solving the coarse grid equations exactly with the Newton method or approximately by performing ν_C smoothing steps. This in contrary to the results obtained in Section 5.1, where we saw a large improvement when the coarse grid problem was solved exactly.

Regarding the hp-multigrid, where we first start with p-multigrid and continue at the lowest polynomial order with h-multigrid, we see that initially there is a significant improvement in reduction of the residual compared to the single-grid computation, but in the asymptotic regime single-grid and hp-multigrid have approximately the same residual reduction per work unit. The reason for this behavior is unclear yet. For the p-multigrid method, initial convergence is significantly faster than for the single-grid computations, but in the asymptotic regime also a comparable convergence history is obtained.

6 Conclusions

Using discrete Fourier analysis, we have analyzed two- and three-level multigrid algorithms for the solution of linear algebraic systems originating from higher order accurate space-time DG discretizations. For the 2D advection-diffusion equation we have shown that by minimizing

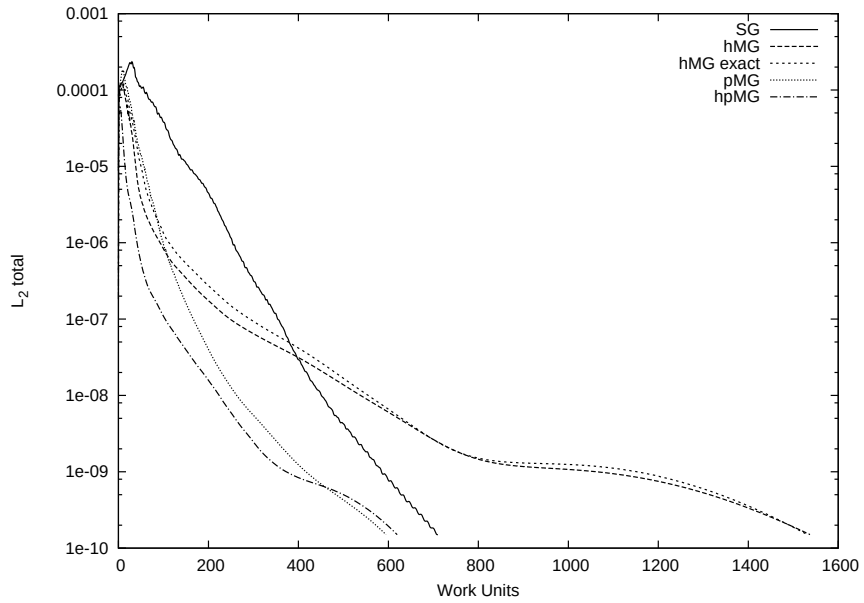

Fig. 4 Convergence history of single-grid, h-, p- and hp-multigrid techniques for the solution of inviscid flow around an NACA0012 airfoil ($\alpha = 2^\circ, Ma = 0.5$).

the spectral radius of the multigrid error transformation operator, a significant improvement in the multigrid performance can be achieved. The algorithms have been tested on a 2D problem containing boundary layers, where the optimized Runge-Kutta smoothers show a significant improvement compared to the original EXI-EXV Runge-Kutta smoother discussed in Ref. 2, 3. Apart from optimizing the multigrid smoother, also the solution of the algebraic system on the coarsest mesh has a big impact on the multigrid performance.

We also compared the performance of h-multigrid with p- and hp-multigrid for solving the Euler equations. We considered subsonic inviscid flow around a NACA0012 airfoil. No significant difference was observed between the EXI scheme and the optimized Runge-Kutta smoothers. The main problem is the deterioration of the convergence rate after the high frequency error modes are smoothed, in particular for h-multigrid. Also, the effect of solving the equations on the coarsest mesh exactly or approximately is small. This in contrast with the 2D advection-diffusion case. Furthermore, we saw that the p- and hp-multigrid methods show a better convergence rate than the h-multigrid method.

References

1. Brandt, A.: Rigorous quantitative analysis of multigrid, I: Constant coefficients two-level cycle with L_2-norm. SIAM J. Numer. Anal. **31**, 1695–1730 (1994).

2. Klaij, C.M., van der Vegt, J.J.W., van der Ven, H.: Pseudo-time stepping methods for space-time discontinuous Galerkin discretizations of the compressible Navier-Stokes equations. J. Comput. Phys. **219**, 622–643 (2006).
3. Klaij, C.M., van Raalte, M.H., van der Ven, H., van der Vegt, J.J.W.: h-Multigrid for space-time discontinuous Galerkin discretizations of the compressible Navier-Stokes equations. J. Comput. Phys. **227**, 1024–1045 (2007).
4. Melson, N.D., Sanetrik, M.D., Atkins, H.L.: Time-accurate Navier-Stokes calculations with multigrid acceleration. in Proc. 6th Copper Mountain Conference on multigrid methods, 423–437, (NASA Langley Research Center 1993)
5. Sudirham, J.J., van der Vegt, J.J.W., van Damme, R.M.J.: Space-time discontinuous Galerkin method for advection-diffusion problems on time-dependent domains. Appl. Numer. Math. **56**, 1491–1518 (2006).
6. Trottenberg, U., Oosterlee, C.W., Schüller, A.: Multigrid. Academic Press, London (2001)
7. van der Vegt, J.J.W., van der Ven, H.: Space-Time Discontinuous Galerkin Finite Element Method with Dynamic Grid Motion for Inviscid Compressible Flows I. General Formulation. J. Comput. Phys. **182**, 546–585 (2002).
8. van der Vegt, J.J.W., Rhebergen, S.: Multigrid optimization using discrete Fourier analysis. Von Karman Institute Lecture Notes (2009)
9. van der Vegt, J.J.W., Rhebergen, S.: Multigrid optimization for higher order accurate space-time discontinuous Galerkin discretizations, in preparation
10. Wesseling, P.: An introduction to multigrid methods. Wiley, Chicester (1991).
11. Wienands, R., Joppich, W.: Practical Fourier analysis for multigrid methods. Chapman & Hall/CRC (2005).
12. Yavneh, I.: Coarse-grid correction for nonelliptic and singular perturbation problems. SIAM J. Sci. Comput. **19**, 1682–1699 (1998).